Applied Physics A (2023) 129:186
https://doi.org/10.1007/s00339-023-06440-4

Applied Physics A
Materials Science & Processing

RAPID COMMUNICATIONS

X-ray emission during the ablative processing of biological materials by ultrashort laser pulses

Sebastian Kraft[1] · Jörg Schille[2] · Jörn Bonse[1] · Udo Löschner[2] · Jörg Krüger[1]

Received: 21 December 2022 / Accepted: 17 January 2023

Abstract
The ablative laser processing with ultrashort pulsed laser beams may cause secondary emission of hazardous X-rays. While the effect has recently been proven to be considered in working safety regulations when processing technical materials, such as metals, the X-ray emission rates during the ablative processing of biological tissue materials are widely unexplored yet. Therefore, biological materials like water, isotonic saline solution, pig eyes, and human teeth were ablated with ultrashort laser pulses of 1030 nm wavelength, 600 fs pulse duration and 5 kHz pulse repetition rate, aiming to mimic typical surgery situations. Simultaneously, *in-situ* X-ray dose rate measurements were performed at a short distance from the plasma to display potential X-ray emission. For all four studied biological materials, our measurements prove the secondary emission of laser-induced X-rays.

Keywords Ultrashort pulsed laser · Laser-induced X-ray emission · Ophthalmology · Dentistry · Secondary hazard · Working safety

1 Introduction

Lasers, especially ultrashort pulsed (usp) lasers, are unique tools for tailored and precise material processing applications [1–4]. Given its enormous societal and commercial relevance, some of the most vivid fields of applications are medicine and esthetic surgery. Since more than 50 years lasers are used in various approaches in medicine [5, 6]. Today, in some of these applications usp laser processing is already involved in the standard therapy, e.g., for refractive vision corrections performed in about 800,000 annual surgeries, just in the USA [7].

When high intensities are involved, particularly for usp lasers, a laser-induced plasma can be generated. It features high electron temperatures that depend on the laser intensity, the pulse duration, the target material and the specific processing conditions. Within the plasma, X-ray photons can be generated due to Bremsstrahlung and characteristic line emission [8–10].

The generation of secondary X-rays by high-intensity laser pulses is known for several decades already [11–13]. Nevertheless, with the rapid development of high-average power usp lasers delivering moderate and high energy ultrashort pulses at MHz pulse repetition rates [14], recently the topic gained attention again in the field of materials processing [15, 16]. It was proven that the laser processing of metals, such as steel and tungsten, can cause hazardous X-ray dose rates that can easily exceed the regulatory safety limits for the operator of the laser processing machines [15–17]. Initial studies on high repetitive laser processing show angle-dependent emission of X-rays with maximal dose rates at an observation angle of about 30° relative to the target surface plane [15].

Regarding practically relevant X-ray dose measurements, one can consider an effective dose for the whole body or organ equivalent doses for partial body exposure, i.e. for the skin. These radiological quantities are defined through X-ray dose equivalents measured at a certain depth of a standardized phantom, namely at a depth of 10 mm for the effective dose $H^*(10)$ and at 0.07 mm depth for the skin dose

✉ Sebastian Kraft
kraft@hs-mittweida.de

✉ Jörg Krüger
joerg.krueger@bam.de

[1] Bundesanstalt für Materialforschung und -prüfung (BAM), Unter den Eichen 87, 12205 Berlin, Germany

[2] Laserinstitut Hochschule Mittweida, University of Applied Sciences Mittweida, Technikumplatz 17, 09648 Mittweida, Germany

Published online: 13 February 2023

$H'(0.07)$. For members of the public, the International Commission on Radiation Units and Measurements recommends dose rate limits of $\dot{H}^*(10) = 1$ mSv/a for the effective dose and $\dot{H}'(0.07) = 50$ mSv/a for the exposure of the skin [18].

While the usp laser-induced hazard has been studied during the last years for various inorganic materials such as metals and glasses [15, 16, 19–21], and for numerous laser irradiation parameters and processing strategies [22–24] in the peak intensity range exceeding 10^{13} W/cm^2, a study of laser-induced X-ray dose rates upon ultrashort pulsed laser processing of biological materials is widely missing. Just very few publications are available, e.g., pointing to the enhancement of the characteristic radiation in X-ray spectra through the additional presence of alkali metal chlorides in aqueous solutions at peak intensities in the range of $2{\cdot}10^{15}$ W/cm^2 [25]. Meesat et al. explored the possibility of cancer radiotherapy based on femtosecond NIR laser-beam direct focusing into the volume of tissue at laser peak intensities between $2.1{\cdot}10^{11}$ W/cm^2 and $3{\cdot}10^{11}$ W/cm^2 yielding high X-ray dose rates of (7.8 ± 0.1) Gy/s [26]. This value equals 2.8 mSv/h dose rate within the tissue at the track of the fs-laser-induced beam filament.

In this work, skin dose rates were measured for four different soft and hard biological tissue materials during ultrashort pulse laser processing in the ablative regime. For all materials, a special emphasis is laid on identifying the focusing conditions causing the maximum X-ray emission rates to allow an initial statement in terms of risks and safety concerns.

2 Laser applications in medicine

Ultrashort pulsed lasers already entered different medical applications for the processing of soft and hard tissue, e.g., in the fields of ophthalmology and dentistry [2, 27].

2.1 Ophthalmology

In eye surgery, ultrashort pulsed lasers are typically used for cutting the cornea, the outer translucent part of the eye. First LASIK (Laser-in-situ-Keratomileusis) eye surgeries were performed in the 1990's with ultraviolet (UV) excimer lasers in combination with a microkeratome, i.e., a precisely cutting metal blade [28]. This blade cuts up the outmost part of the cornea (containing nerves) and generates the so-called "flap". After moving the flap aside, UV-laser processing reshaped the exposed inner part of the cornea for individually optimized visual correction. Subsequently, the flap is repositioned, covering the laser-treated surface. In the further development of the LASIK technique, the initial cutting of the flap by mechanical blades was substituted with an usp laser process, taking benefit of this fully contactless and sterile flap-cutting method [29, 30]. At laser intensities of $\approx 10^{11}$ W/cm^2 the optical breakdown in the corneal tissue is used to generate pronounced cavities on the micrometer scale. The spot-by-spot laser perforation significantly enhanced the achievable performance, precision, and quality of the entire flap-cutting process. The femto-LASIK is nowadays a standard treatment for the correction of myopia, hyperopia, and astigmatism. Other modern laser-surgeries like the SMILE (Small Incision Lenticule Extraction) treatment are an all-fs-laser solution without the UV-excimer laser source and flap creation [31]. To further increase the quality, approaches with finer laser focusing and lower pulse energies are tested and show good results. The smaller laser-induced cavities lower the processed tissue roughness and reduce the limits for flap thickness. Besides such visual corrections, ultrashort lasers are also used for cuts in the cornea for keratoplasty and cataract surgery [32].

On the laser side two main approaches, the low and high pulse energy regime, are used with slightly different parameters. In the "high energy regime", laser pulse energies up to 15 µJ, in eye surgery about 1 µJ, and a beam diameter of typically 30 µm are used. In the "low energy regime" only about 100 nJ pulse energy with smaller focal spot diameters of ≈ 2 µm are utilized. In both cases, the peak intensity in clinical application is $\approx 5{\cdot}10^{13}$ W/cm^2 [33]. The wavelength of the laser radiation of 1030 nm and pulse durations of 300–800 fs is currently the standard of most laser systems admitted in medical applications [34].

2.2 Dentistry

In dentistry, the teeth are reshaped for reconstruction purposes with lasers for decades. As an example, Niemz et al. [35] demonstrated improved quality in dental enamel processing when using ultrashort laser pulses instead of pulses of longer pulse durations. The small heat-affected zone and a specific selectivity between the removal of healthy or caries-affected material enables a new field of application in dentistry. On the one hand, a low ablation rate of the hard tooth materials, enamel and dentin, leads to a long treatment time for the patients if low repetition rate (few kHz) lasers are involved. On the other hand, higher laser pulse energies and fluences or heat-accumulation effects at high laser pulse repetition rates in the hundreds of kHz to MHz range raise the risk of pain on the patient side due to the generation of heat or may even generate thermally induced microcracks [36–38]. Such cracks can be an issue for additional caries growth. Therefore, the used laser pulse energies and intensity is limited to a certain value. The highest ablation efficiency of tooth materials

and restoration materials has been reported in the fluence range between 5 and 10 J/cm^2 [39, 40]. This corresponds to peak intensities of about $3{\cdot}10^{13}$ W/cm^2 for a fluence of 10 J/cm^2 and a pulse duration of 300 fs.

3 Methods

As described above, ultrashort laser pulses of $5{\cdot}10^{13}$ W/cm^2 maximum peak intensity and near-infrared laser wavelength (around 1 µm) are used in medicine. The beam focal spot diameter in ophthalmology can be as small as 0.5 µm. To match these requirements as good as possible the experimental set-up sketched in Fig. 1 is used here.

The experiments were performed in a safety enclosure for protection against possible X-rays. Inside the clean room laboratory, room temperature and humidity were kept constant. The used laser beam source was an Edgewave FX200 (Edgewave GmbH, Germany) InnoSlab amplifier system with a center wavelength of 1030 nm, a pulse duration of 600 fs, and a maximal pulse energy of 35 µJ. After travelling through a 3× expanding telescope, the enlarged laser beam was focused by an aspheric lens of 80 mm focal length. The aspheric lens facilitates less distortions than a spherical lens at lower focal distances for achieving smaller focused beam spot size.

As another advantage, the 80 mm focal length enables the usage of a protecting optical window between the specimen and the focusing lens to avoid both contaminations of the lens with ablation products and shielding of X-ray radiation propagating to the detector´s surface. To measure X-ray emission dose rates, a dosimeter OD-02 (Step Sensortechnik und Elektronik Pockau GmbH, Germany) was used. The distance between the point of the laser-matter interaction and the dosimeter was about 15 cm at 30° angle of incidence with reference to the sample surface.

After fine adjustment of the laser beam focusing, the caustic of the focused beam was measured with a beam profiler MicroSpotMonitor 25 (Primes GmbH, Germany) to identify the energy distribution within the laser spot in different planes after the lens. With this caustic measurement, the intensity distributions in the z-planes could be numerically calculated.

In these calculations, a pulse duration of 600 fs (sech^2) and a total laser pulse energy of (35.5 ± 0.8) µJ were taken into account. Accordingly, the peak intensity in the focal plane was $I_0 = I(x=0,\ y=0) = (7.8 \pm 0.6){\cdot}10^{13}$ W/cm^2, as shown in Fig. 1 (left). The z-axis moving stage allowed relative movement between the specimen surface and focal plane. With a greater distance of the specimen surface from the focal plane (± 220 µm), the peak intensity reduces from $7.8{\cdot}10^{13}$ W/cm^2 to $1{\cdot}10^{13}$ W/cm^2 as depicted in Fig. 2.

The specimens were placed by an xy-axis translation system under the focusing optics. To realize identical conditions for each experiment, the same program routine for the laser irradiations was executed. The laser pulses were triggered by the position-synchronized output (PSO) signal of the xy -axis system. The fact that liquids were used as a specimen in some cases, a slow processing speed of 5 mm/s was chosen to avoid liquid movement. In each experiment, the laser irradiation was performed in a meandering way processing an area of 5 × 5 mm^2 with an intra-line pulse distance of 1 µm and an inter-line separation of 20 µm. This resulted in a pulse repetition rate of 5 kHz and an average laser power

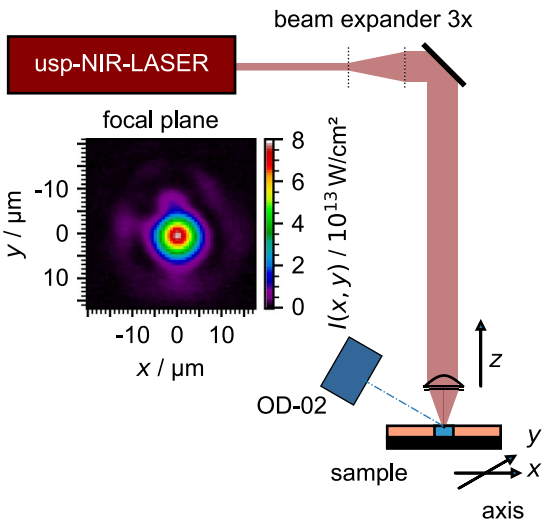

Fig. 1 Scheme of the experimental set-up for laser-induced X-ray generation with a 3×expanded near-infrared ultrashort pulsed laser beam focused through an aspherical lens along with the measured intensity distribution $I(x, y, z=z_{foc})$ at the focal plane. X-ray dose rates were measured under an angle of 30° to the sample surface at 15 cm distance from the laser-processed spot using an OD-02 detector

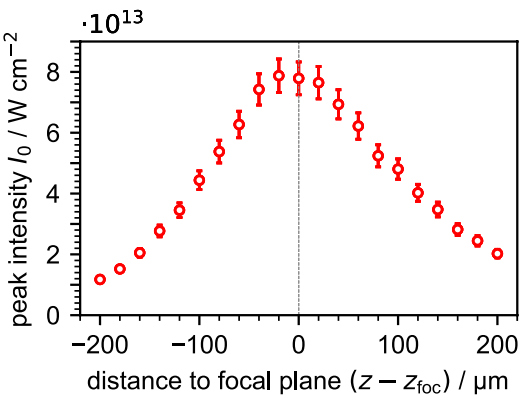

Fig. 2 Numerically calculated peak intensity as a function of the distance between the focal plane and z-position. The maximal overall peak intensity at the focus position of the laser beam z_{foc} is $7.8{\cdot}10^{13}$ W/cm^2

of (178 ± 5) mW. This low laser power led to a low thermal heat load of the specimen. To determine if the measured X-ray dose rates were naturally based or of laser-induced origin, the natural background X-ray radiation was measured in the laboratory without laser irradiation. For that, the background signal was monitored for one hour showing $\dot{H}'(0.07)_{BG} = (0.08 \pm 0.06)$ µSv/h (2σ). Within the one-hour measurement of the stochastic natural-based radiation little peaks occur with a maximum dose rate of up to 0.22 µSv/h, which are not included within the standard variance 2σ.

4 Results

Three different representative material classes were investigated. These are liquids representing soft tissue, water and isotonic saline solution, and pig eyes and human teeth as model systems in ophthalmology and dentistry, respectively. The pig eyes used in the presented work were preserved in form of unscalded animal byproducts harvested by veterinary services. The pig eyes were transported in a humidified box and laser processed 30 min after removal to maintain unadulterated conditions of the biological tissue. The human teeth from patients were delivered by a local dentist. In the time lapse between tooth pulling from a human patient and laser processing, the extracted teeth were stored in a formalin solution. This was done to comply with hygienic and health protection standards and further to avoid dehydration of the tooth specimen.

4.1 Soft tissue models

The human body's main component (68%) [41] is water or saline solution. Therefore, these two liquids are suitable materials representing simple models of soft tissue. In the experiments tap water H_2O and isotonic saline solution NaCl(aq) (0.9%) (Serumwerk Bernburg, Germany) were used.

The liquids were filled into small containers (40 ml) being open at the top and placed below the laser processing optics. The focal plane was shifted stepwise ($dz = 20$ µm) after every complete scan execution on a 5×5 mm^2 sized area. The measurements started 200 µm underneath liquids' surface moving upwards until reaching 200 µm position above the liquids' surface. This technique allows us to find the best overlap of liquids' surface at $z_{surface}$ and focal plane, where the X-ray emission is assumed maximal. The approach can consider that the surface level of the liquid changed due to laser-induced evaporation, little movement of the liquids, laser ablation pressure and somewhat different filling level of the containers.

The laser-induced X-ray emissions recorded at different focal plane distances, Fig. 3, are considerably above

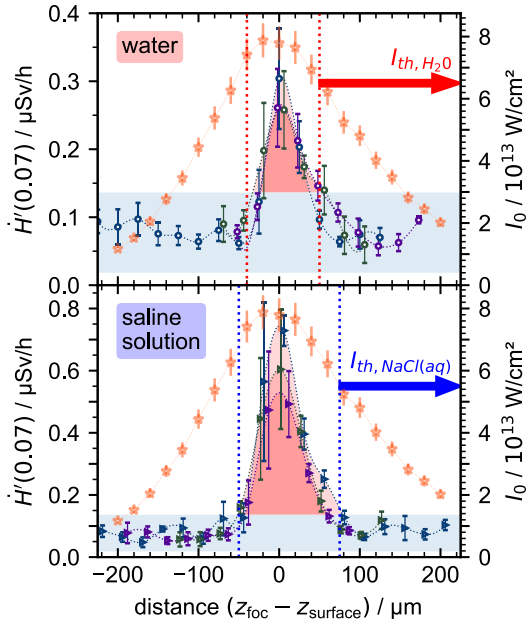

Fig. 3 Laser-induced X-ray skin dose rates $\dot{H}'(0.07)$ measured at different focal positions to the surface and corresponding peak intensities at the surface I_0 (orange stars) at soft tissue representatives water H_2O (top panel, circles) and isotonic saline solution NaCl(aq) (bottom panel, triangles) for three experiments, blue, green and violet. The light blue area indicates the natural background radiation dose rate (2σ)

X-ray background radiation within the studied parameter range. The graphs of the repeated experiments are leveled so that the highest emission occurs at $z_{foc} = z_{surface}$. The laser-induced X-ray emission, indicated red shaded in Fig. 3, exceeds the natural X-ray background radiation, 2σ-referenced with the blue shaded area in Fig. 3, while processing with the laser beam focal plane near the liquids' surface.

Although the detected maximum X-ray dose rate values vary from one laser irradiation procedure to the other, a clear correlation between the maximum dose rate and the highest laser peak intensity can be seen at the z-axis focus position. Therefore, is it very likely, that the detected X-ray emission originated not from statistic natural X-ray emissions but rather from the laser process. The maximum X-ray emission dose rates were measured as $\dot{H}'(0.07)_{H_2O/max} = (0.32 \pm 0.07)$ µSv/h for water and $\dot{H}'(0.07)_{NaCl(aq)/max} = (0.76 \pm 0.05)$ µSv/h for isotonic saline solution. Both values are clearly above the detected X-ray background radiation of 0.22 µSv/h. In addition, the effective dose rate $\dot{H}^*(10)$ was analyzed in the experiments, however, the values could not clearly be distinguished from the natural background level here. This points toward X-ray photon emissions in the soft X-ray range, which are strongly absorbed by soft tissue (water).

With the knowledge of the peak intensity distribution along the z-axis, see Fig. 2, the threshold intensity I_{th} for

the start of the laser-induced X-ray emission can be figured out for the different irradiated biological materials. Accordingly, in Fig. 3, two horizontal (colored) arrows project the lower limit of detectable laser-induced skin dose rates to the corresponding peak intensity value. The usp laser intensity threshold is $6.5{\cdot}10^{13}$ W/cm^2 for water and $5.5{\cdot}10^{13}$ W/cm^2 for the isotonic saline solution here.

4.2 Ophthalmological model

Pig eyes were selected as representative material in ophthalmology. They have been proven to be a good replacement model for human eyes or corneas in experimental studies due to their great similarity [42, 43]. The unscalded life-like pig eyes were placed inside a specially designed holder below the focusing optics. Due to the curved surface shape of the cornea, three experiments with different processing strategies were performed. The first experiment (procedure #1) was conducted with different focal plane positions, like in the experiments performed with the liquids and linear z-axis movement. The second strategy (procedure #2) involves a constant focal position at one z-position and a linear movement of the eye along a direction perpendicular to the beam direction while monitoring the X-ray emission. In the third approach (procedure #3), a circular eye movement at a constant focal z-position was realized during the dose rate measurements. In all regimes, the focal position was reached at one specific time at the cornea surface, where the maximal laser intensity $I_0 = 7.8{\cdot}10^{13}$ W/cm^2 is used for ablation.

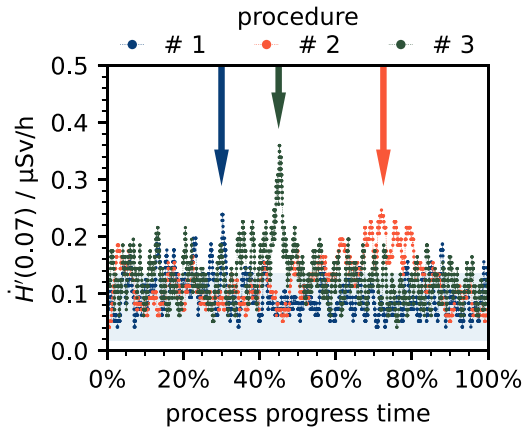

Fig. 4 Temporal variation during the X-ray skin dose rate measurements, while performing three different processing procedures with pig eyes as a model specimen for ophthalmological applications with a peak intensity $I_0 = (7.8 \pm 0.6){\cdot}10^{13}$ W/cm^2. The light blue area indicates the natural background radiation dose rate (2σ). The procedures are #1: linear processing with increasing focal position, #2: linear processing with a constant focal position and #3: circular movement with a constant focal position. The arrows indicate the times with additional laser-induced X-ray exposure

As indicated in Fig. 4 by vertical arrows, clear peaks of X-ray emissions above the background X-ray emission dose level are distinguishable in all three measurements. Noteworthy, the maximum value assessed for the laser-induced dose rate was of about the same level as figured out for laser processing in water. Hence, with a percentage of approximately 78% of water, the cornea's main component is water and, therefore, these results are in reasonable agreement.

After the laser treatment of three different pig eyes, all corneas showed severe damage and the laser-irradiated areas appeared blurred. This might be due to the fact that the applied laser peak intensities are set at a too high level in comparison with realistic irradiation conditions in clinical surgery. Therefore, the experiments were repeated with two lower peak intensities, $I_0 = (6.0 \pm 0.6){\cdot}10^{13}$ W/cm^2 and $I_0 = (4.0 \pm 0.6){\cdot}10^{13}$ W/cm^2, compared to the maximum intensity $I_0 = (7.8 \pm 0.6){\cdot}10^{13}$ W/cm^2 applied in the initial experiments. At these lower peak intensity levels, no X-ray emission above the natural background X-ray dose rate could be observed.

4.3 Dentistry model

In a third set of experiments, X-ray emissions arising from laser processing of human tooth material are studied. The laser processed tooth's components are mainly enamel, the outer layer of a tooth, and dentin, its inner constituent. On the laser processing side, these two materials behave slightly different in terms of ablation rate and ablation threshold [39]. For better handling, the teeth were embedded in epoxy resin and subsequently mechanically ground. The flat cross-sections exhibit the two named tooth materials, dentin and enamel, at the sample surface.

Additionally, to avoid misreading the detector signals, the epoxy resin was tested with respect to laser-induced X-ray emission at the used laser parameters. No significant X-ray emission exceeding the natural background level could be detected for the epoxy resin at the selected laser peak intensities.

Due to the natural shape of the teeth, the 5×5 mm^2 laser-processed areas, were not fully covered with only one tooth component which potentially affects the X-ray emission dose rate. As done before in water, in saline solution and by studying pig eyes, the tooth specimens were laser processed by varying the position of the laser focus spot relatively to the specimen surface, see Fig. 5. In total, six newly polished tooth cross sections were used.

The X-ray emission varied during the repeated experiments with new tooth material. The measured dose rate varied locally depending on the percentage of enamel, dentin and epoxy per processed ablation line, which is indicated by the large error bars in Fig. 5 of the X-ray emission dose values monitored in the repeated experiments. The intensity

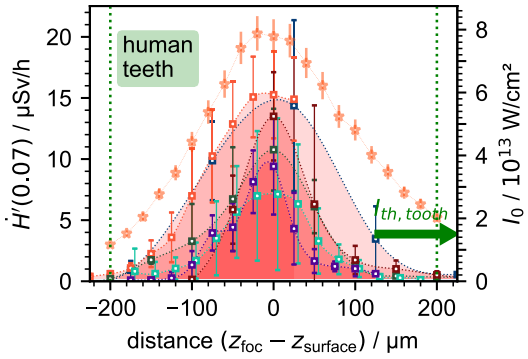

Fig. 5 Laser-induced X-ray generation of embedded human teeth during laser ablation processing series conducted at six tooth cross-sections (squares) with different focal to surface distances and resulting peak intensities (orange stars)

threshold for laser-induced X-ray generation in tooth material can be estimated from the curves in Fig. 5 as about $I_{th} = 1.5–3 \cdot 10^{13}$ W/cm^2. In accordance with the results presented above for studying the effective dose rate $\dot{H}^*(10)$, no noticeable increase in the dose rate level above the natural background radiation was detected here. Therefore, it can be assumed that soft X-rays with photon energies below 10 keV are generated.

5 Discussion

Our results show that it is possible to generate laser-induced X-ray emissions with a sub-ps NIR laser beam focused to a peak intensity of $I_0 = (7.8 \pm 0.6) \cdot 10^{13}$ W/cm for all representative biological materials.

For water, saline solution, and pig eyes the peak intensity threshold for laser-induced generation of X-ray emissions exceeding the natural background level is in the range of $5–7 \cdot 10^{13}$ W/cm^2. The X-ray skin dose rates $\dot{H}'(0.07)$ arising from repeated laser irradiations at 5 kHz pulse repetition rate and 178 mW average laser power were measured in the range between 0.3 and 0.8 µSv/h, which could be clearly distinguished from the natural background.

Besides the soft tissue representatives, ultrashort pulsed laser ablation of human teeth was investigated for potential laser-induced X-ray generation. The experimental data reveal a relatively low laser intensity threshold of about $I_{th} = 1.5–3 \cdot 10^{13}$ W/cm^2. Here, X-ray skin dose rates $\dot{H}'(0.07)$ up to 20 µSv/h were measured.

Our results show a possible X-ray exposure for the patients, the surgeons and medical assistants during a laser-assisted operation. As a legal limit, an annual skin dose of 50 mSv is allowed for the general public.

On the patient side, the duration of the X-ray-producing processes per year can be reduced to a few minutes or less. The highest X-ray exposure is obtained while laser-processing the teeth, therefore the dose rates for dentistry are estimated. The distance between healthy tissue, gums or cheeks, and the laser-generated plasma at the teeth representing the X-ray source, is typically around 1 cm. Due to this considerably lower distance as in the above-discussed experiments, the dose rate will increase by a factor of about 250 compared to the effective X-ray dose rate at a 15 cm distance. As a consequence, a skin dose rate of approx. 5 mSv/h at 1 cm distance must be considered in the risk assessment. The annual limit will be reached after 10 h of laser processing in this case.

Due to the larger distances for the surgeons and medical assistants from the source of X-ray generation, the circumstances are different from that for the patient. By estimating an 8 h workday with 25% of laser processing on 200 working days per year, a total of 400 h of possible X-ray exposure can arise. The distance of the operator's hand to the X-ray source can be estimated to be about 10 cm, increasing the dose rate by a factor of about 2.5, reaching 50 µSv/h at this position. Thus, the annual X-ray dose affecting the operator's fingers accumulates up to 20 mSv, close to half of the annual exposure limit.

Another fact worth mentioning is that laser treatment has been assessed based on a low average laser power of 178 mW, a moderate repetition rate of 5 kHz, and intensities close to literature values here. In reality, higher average power and/or pulse repetition rates might be utilized. Therefore, the conclusions are limited to the laser parameters used in this study.

6 Conclusion

In-situ X-ray dose rate measurements were performed during ultrashort pulse laser treatment of soft and hard biological materials with a wavelength of 1030 nm, a pulse duration of 600 fs, a pulse repetition rate of 5 kHz, and an average laser power of 178 mW. For water, isotonic saline solution, and pig eyes X-ray skin dose rates below 1 µSv/h were measured clearly distinguishable from the natural background. During laser ablation of human teeth, X-ray skin dose rates up to 20 µSv/h were monitored at a 15 cm distance from the laser-irradiation area.

Acknowledgements We thank the dentist Mrs. Marion Riede (Zahnarztpraxis Seifert, Geithain, Germany) for providing the dental material used in the study.

Author contributions Conceptualization: SK, UL, JK; Methodology, Data curation, Formal analysis and investigation: SK;

Writing—original draft preparation: SK; Writing—JS, JB, JK; Review and editing: SK, JS, JB, JK; Funding acquisition: UL, JK; Resources: JS; Project administration: UL, JK.

Funding Open Access funding enabled and organized by Projekt DEAL. This research was funded by the German Federal Office for Radiation Protection (BfS), grant number 3621S42451.

Data availability The datasets generated during and/or analysed during the current study are available from the corresponding author on reasonable request.

Declarations

Ethical approval The used biological materials, veterinary-tested pig eyes and sanitized human teeth, were all provided by professionals. These materials are byproducts and not harvested for this purpose and non-retraceable.

References

1. D. Bäuerle, *Laser processing and chemistry*, 4th edn. (Springer, Berlin, 2011). https://doi.org/10.1007/978-3-642-17613-5
2. F. Dausinger, F. Lichtner, H. Lubatschowski (eds.), *Femtosecond technology for technical and medical applications* (Springer, Berlin, 2004)
3. K. Sugioka, Y. Cheng (eds.), *Ultrafast laser processing: from micro- to nanoscale industrial applications* (Taylor & Francis Group, Boca Raton, 2013)
4. R. Stoian, J. Bonse (eds.), *Ultrafast laser nanostructuring—the pursuit of extreme scales* (Springer Nature, Cham, 2023). (**In press**)
5. T.G. Polanyi, H.C. Bredemeier, T.W. Davis Jr., A CO_2 laser for surgical research. Med. Biol. Eng. **8**, 541–548 (1970). https://doi.org/10.1007/BF02478228
6. Q. Peng, A. Juzeniene, J. Chen, L.O. Svaasand, T. Warloe, K.-E. Giercksky, J. Moan, Lasers in medicine. Rep. Progr. Phys. **71**, 056701 (2008). https://doi.org/10.1088/0034-4885/71/5/056701
7. S.N. Joffe, The 25th anniversary of laser vision correction in the United States. Clin. Ophthalmol. **15**, 1163–1172 (2021). https://doi.org/10.2147/OPTH.S299752
8. H. Legall, J. Bonse, J. Krüger, Review of X-ray exposure and safety issues arising from ultra-short pulse laser material processing. J. Radiol. Prot. **41**, R28–R42 (2021). https://doi.org/10.1088/1361-6498/abcb16
9. J. Holland, R. Weber, M. Sailer, C. Hagenlocher, T. Graf, Pulse duration dependency of the X-ray emission during materials processing with ultrashort laser pulses. Procedia CIRP **111**, 855–858 (2022). https://doi.org/10.1016/j.procir.2022.08.097
10. K. Böttcher, M. Schmitt Rahner, U. Stolzenberg, S. Kraft, J. Bonse, C. Feist, D. Albrecht, B. Pullner, J. Krüger, Worst-case X-ray photon energies in ultrashort pulse laser processing. Materials **15**, 8996 (2022). https://doi.org/10.3390/ma15248996
11. M.M. Murnane, H.C. Kapteyn, M.D. Rosen, R.W. Falcone, Ultrafast X-ray pulses from laser-produced plasmas. Science **251**, 531–536 (1991). https://doi.org/10.1126/science.251.4993.531
12. J. Thogersen, A. Borowiec, H.K. Haugen, F.E. McNeill, I.M. Stronach, X-ray emission from femtosecond laser micromachining. Appl. Phys. A **73**, 361–363 (2001). https://doi.org/10.1007/s003390100741
13. J. Bunte, S. Barcikowski, T. Puester, T. Burmester, M. Brose, T. Ludwig, Secondary hazards: particle and X-ray emission, in *Femtosecond technology for technical and medical applications*. ed. by F. Dausinger, H. Lubatschowski, F. Lichtner (Springer, Berlin, 2004). https://doi.org/10.1007/978-3-540-39848-6_20
14. J. Schille, U. Loeschner, Ultrashort pulse lasers in high-rate laser micro processing—Quo vadis? Adv. Opt. Technol. **10**, 233–237 (2021). https://doi.org/10.1515/aot-2021-049
15. H. Legall, C. Schwanke, S. Pentzien, G. Dittmar, J. Bonse, J. Krüger, X-ray emission as a potential hazard during ultrashort pulse laser material processing. Appl. Phys. A **124**, 407 (2018). https://doi.org/10.1007/s00339-018-1828-6
16. R. Behrens, B. Pullner, M. Reginatto, X-ray emission from materials processing lasers. Radiat. Prot. Dosim. **183**, 361–374 (2019). https://doi.org/10.1093/rpd/ncy126
17. H. Legall, C. Schwanke, J. Bonse, J. Krüger, X-ray radiation protection aspects during ultrashort laser processing. J. Laser Appl. **32**, 022004 (2020). https://doi.org/10.2351/1.5134778
18. 1990 Recommendations of the International Commission on Radiological Protection. ICRP Publication 60. Ann. ICRP Vol. **21** No. 1–3 (1991). https://www.icrp.org/publication.asp?id=icrp%20publication%2060. Accessed 20 Dec 2022
19. P. Mosel, P. Sankar, Zulqarnain, E. Appi, C. Jusko, D. Zuber, S. Kleinert, J. Düsing, J. Mapa, G. Dittmar, T. Püster, P. Böhmer-Brinks, J.-W. Vahlbruch, U. Morgner, M. Kovacev, Potential hazards and mitigation of X-ray radiation generated by laser-induced plasma from research-grade laser systems. Opt. Express **30**, 37038–37050 (2022). https://doi.org/10.1364/OE.468135
20. R. Weber, R. Giedl-Wagner, D.J. Förster, A. Pauli, T. Graf, J.E. Balmer, Expected X-ray dose rates resulting from industrial ultrafast laser applications. Appl. Phys. A **125**, 635 (2019). https://doi.org/10.1007/s00339-019-2885-1
21. J. Schille, S. Kraft, D. Kattan, U. Löschner, Enhanced X-ray emissions arising from high pulse repetition frequency ultrashort pulse laser materials processing. Materials **15**, 2748 (2022). https://doi.org/10.3390/ma15082748
22. H. Legall, C. Schwanke, J. Bonse, J. Krüger, The influence of processing parameters on X-ray emission during ultra-short pulse laser machining. Appl. Phys. A **125**, 570 (2019). https://doi.org/10.1007/s00339-019-2827-y
23. J. Schille, S. Kraft, T. Pflug, C. Scholz, M. Clair, A. Horn, U. Loeschner, Study on X-ray emission using ultrashort pulsed lasers in materials processing. Materials **14**, 4537 (2021). https://doi.org/10.3390/ma14164537
24. D. Metzner, M. Olbrich, P. Lickschat, A. Horn, S. Weißmantel, X-ray generation by laser ablation using MHz to GHz pulse bursts. J. Laser Appl. **33**, 032014 (2021). https://doi.org/10.2351/7.0000403
25. K. Hatanaka, T. Miura, H. Fukumura, Ultrafast X-ray pulse generation by focusing femtosecond infrared laser pulses onto aqueous solutions of alkali metal chloride. Appl. Phys. Lett. **80**, 3925 (2002). https://doi.org/10.1063/1.1482135
26. R. Meesat, H. Belmouaddine, J.-F. Allard, C. Tanguay-Renaud, R. Lemay, T. Brastaviceanu, L. Tremblay, B. Paquette, J.R. Wagner,

J.-P. Jay-Gerin, M. Lepage, M.A. Huels, D. Houde, Cancer radiotherapy based on femtosecond IR laser-beam filamentation yielding ultra-high dose rates and zero entrance dose. PNAS **109**, 2508–2513 (2012). https://doi.org/10.1073/pnas.1116286109
27. M.H. Niemz, *Laser tissue interactions—fundamentals and applications*, 3rd edn. (Springer, Berlin, 2007). https://doi.org/10.1007/978-3-540-72192-5
28. I.G. Pallikaris, M.E. Papatzanaki, E.Z. Stathi, O. Frenschock, A. Georgiadis, Laser in situ keratomileusis. Lasers Surg. Med. **10**, 463–468 (1990). https://doi.org/10.1002/lsm.1900100511
29. H. Lubatschowski, G. Maatz, A. Heisterkamp, U. Hetzel, W. Drommer, H. Welling, W. Ertmer, Application of ultrashort laser pulses for intrastromal refractive surgery. Graefe's Arch. Clin. Exp. Ophthalmol. **238**, 33–39 (2000). https://doi.org/10.1007/s004170050006
30. I. Ratkay-Traub, I.E. Ferincz, T. Juhasz, R.M. Kurtz, R.R. Krueger, First clinical results with the femtosecond Neodymium-glass laser in refractive surgery. J. Refract. Surg. **19**, 94–103 (2003). https://doi.org/10.3928/1081-597X-20030301-03
31. W. Sekundo, *Small Incision Lenticule Extraction (SMILE)* (Springer, Cham, 2015). https://doi.org/10.1007/978-3-319-18530-9
32. B. Pajic, Z. Cvejic, B. Pajic-Eggspuehler, Cataract surgery performed by high frequency LDV Z8 femtosecond laser: safety, efficacy, and its physical properties. Sensors **17**, 1429 (2017). https://doi.org/10.3390/s17061429
33. M. Tomita, Y. Sotoyama, S. Yukawa, T. Nakamura, Comparison of DLK incidence after laser in situ keratomileusis associated with two femtosecond lasers: Femto LDV and IntraLase FS60. Clin. Ophthalmol. **7**, 1365–1371 (2013). https://doi.org/10.2147/opth.s47341
34. T. Asshauer, C. Latz, A. Mirshahi, C. Rathjen, Femtosecond lasers for eye surgery applications: historical overview and modern low pulse energy concepts. Adv. Opt. Technol. **10**, 393–408 (2021). https://doi.org/10.1515/aot-2021-0044
35. M.H. Niemz, Investigation and spectral analysis of the plasma-induced ablation mechanism of dental hydroxyapatite. Appl. Phys. B **58**, 273–281 (1994). https://doi.org/10.1007/BF01082621
36. M. Bello-Silva, M. Wehner, C. Eduardo, F. Lampert, R. Poprawe, M. Hermans, M. Esteves-Olivera, Precise ablation of dental hard tissues with ultra-short pulsed lasers. Preliminary exploratory investigation on adequate laser parameters. Lasers Med. Sci. **28**, 171–184 (2013). https://doi.org/10.1007/s10103-012-1107-2
37. J. Krüger, W. Kautek, H. Newesely, Femtosecond-pulse laser ablation of dental hydroxyapatite and single-crystalline fluoroapatite. Appl. Phys. A **69**(Suppl), S403–S407 (1999). https://doi.org/10.1007/s003399900215
38. A. Braun, R.J. Wehry, O. Brede, C. Dehn, M. Frentzen, F. Schelle, Heat generation caused by ablation of restorative materials with an ultrashort pulse laser (USPL) system. Lasers Med. Sci. **27**, 297–303 (2012). https://doi.org/10.1007/s10103-010-0875-9
39. F. Schelle, S. Polz, H. Haloui, A. Braun, C. Dehn, M. Frentzen, J. Meister, Ultrashort pulsed laser (USPL) application in dentistry: basic investigations of ablation rates and thresholds on oral hard tissue and restorative materials. Lasers Med. Sci. **29**, 1775–1783 (2014). https://doi.org/10.1007/s10103-013-1315-4
40. S. Loganathan, S. Santhanakrishnan, R. Bathe, M. Arunachalam, Surface processing: an elegant way to enhance the femtosecond laser ablation rate and ablation efficiency on human teeth. Lasers Surg. Med. **51**, 797–807 (2019). https://doi.org/10.1002/lsm.23105
41. H.H. Mitchell, T.S. Hamilton, F.R. Steggerda, H.W. Bean, The chemical composition of the adult human body and its bearing on the biochemistry of growth. JBC **158**, 625–637 (1945). https://doi.org/10.1016/S0021-9258(19)51339-4
42. P.G. McMenamin, R.J. Steptoe, Normal anatomy of the aqueous humour outflow system in the domestic pig eye. J. Anat. **178**, 65–77 (1991). (PMCID: PMC1260535)
43. M. Crespo-Moral, L. Garcia-Posadas, A. Lopez-Garcia, Y. Diebold, Histological and immunohistochemical characterization of the porcine ocular surface. PLoS ONE **15**, e0227732 (2020). https://doi.org/10.1371/journal.pone.0227732